Gallium 68 PSMA-11 PET/MR Imaging in Patients with Intermediate- or High-Risk Prostate Cancer

Sonya Youngju Park, MD • *Claudia Zacharias, MD* • *Caitlyn Harrison, MD* • *Richard E. Fan, PhD* • *Christian Kunder, MD, PhD* • *Negin Hatami, MD* • *Frederik Giesel, MD* • *Pejman Ghanouni, MD, PhD* • *Bruce Daniel, MD* • *Andreas M. Loening, MD, PhD* • *Geoffrey A. Sonn, MD* • *Andrei Iagaru, MD*

From the Division of Nuclear Medicine and Molecular Imaging (S.Y.P., C.Z., C.H., N.H., A.I.) and Departments of Urology (R.E.F., G.A.S.), Pathology (C.K.), and Radiology (P.G., B.D., A.M.L.), Stanford University Medical Center, 300 Pasteur Dr, Room H-2200, Stanford, CA 94305; and Department of Nuclear Medicine, University Hospital Heidelberg, Heidelberg, Germany (F.G.). Received September 21, 2017; revision requested November 1; accepted February 12, 2018. **Address correspondence to** A.I. (e-mail: *aiagaru@stanford.edu*).

Study supported by GE Healthcare.

Conflicts of interest are listed at the end of this article.

Radiology 2018; ▬:1–11 • https://doi.org/10.1148/radiol.2018172232 • Content codes: GU NM MI OI

Purpose: To report the results of dual-time-point gallium 68 (^{68}Ga) prostate-specific membrane antigen (PSMA)-11 positron emission tomography (PET)/magnetic resonance (MR) imaging prior to prostatectomy in patients with intermediate- or high-risk cancer.

Materials and Methods: Thirty-three men who underwent conventional imaging as clinically indicated and who were scheduled for radical prostatectomy with pelvic lymph node dissection were recruited for this study. A mean dose of 4.1 mCi ± 0.7 (151.7 MBq ± 25.9) of ^{68}Ga-PSMA-11 was administered. Whole-body images were acquired starting 41–61 minutes after injection by using a GE SIGNA PET/MR imaging unit, followed by an additional pelvic PET/MR imaging acquisition at 87–125 minutes after injection. PET/MR imaging findings were compared with findings at multiparametric MR imaging (including diffusion-weighted imaging, T2-weighted imaging, and dynamic contrast material–enhanced imaging) and were correlated with results of final whole-mount pathologic examination and pelvic nodal dissection to yield sensitivity and specificity. Dual-time-point metabolic parameters (eg, maximum standardized uptake value [SUV_{max}]) were compared by using a paired *t* test and were correlated with clinical and histopathologic variables including prostate-specific antigen level, Gleason score, and tumor volume.

Results: Prostate cancer was seen at ^{68}Ga-PSMA-11 PET in all 33 patients, whereas multiparametric MR imaging depicted Prostate Imaging Reporting and Data System (PI-RADS) 4 or 5 lesions in 26 patients and PI-RADS 3 lesions in four patients. Focal uptake was seen in the pelvic lymph nodes in five patients. Pathologic examination confirmed prostate cancer in all patients, as well as nodal metastasis in three. All patients with normal pelvic nodes in PET/MR imaging had no metastases at pathologic examination. The accumulation of ^{68}Ga-PSMA-11 increased at later acquisition times, with higher mean SUV_{max} (15.3 vs 12.3, $P < .001$). One additional prostate cancer was identified only at delayed imaging.

Conclusion: This study found that ^{68}Ga-PSMA-11 PET can be used to identify prostate cancer, while MR imaging provides detailed anatomic guidance. Hence, ^{68}Ga-PSMA-11 PET/MR imaging provides valuable diagnostic information and may inform the need for and extent of pelvic node dissection.

Online supplemental material is available for this article.

The American Cancer Society projects that in 2017, prostate cancer will remain the leading noncutaneous cancer diagnosed in American males, with 161 360 estimated new cases and 26 730 deaths (1). Initial screening and diagnosis relies on the digital rectal examination, serum prostate-specific antigen (PSA) testing, and transrectal ultrasonography (US)-guided biopsies (2,3). Depending on cancer stage and grade, treatment may involve observation, surgery (prostatectomy), radiation therapy (external beam or brachytherapy), hormonal therapy, chemotherapy, or a combination of these (4–6).

The use of multiparametric magnetic resonance (MR) imaging is increasing rapidly because of its ability to improve detection of clinically important index tumors (7). The choice of treatment directly depends on the initial stage, which is based on the TNM classification. Guidelines vary, but in general, men with a T stage greater than 2, a PSA level greater than 20 ng/mL, or a Gleason score of 8 or greater require staging with bone scanning and pelvic computed tomographic (CT) or MR imaging (8). CT or MR imaging is primarily used to identify local-regional lymph nodes (thereby altering the N stage), while the bone scan is primarily used to identify osseous metastatic disease (thereby altering the M stage). However, CT, MR imaging, and bone scanning have limited accuracy in depicting retroperitoneal small lymph node metastases that do not trigger size criteria at CT and MR imaging and small-volume bone metastases. In fact, pathologic evaluation is not only frequently associated with upstaging of clinical disease, but clinical outcomes also vary greatly among different patients with the same pathologic stage disease (9).

Molecular imaging has great potential to improve prostate cancer staging. Prostate-specific membrane antigen (PSMA) is a cell surface protein that is markedly overexpressed in prostate cancer cells when compared with other PSMA-expressing tissues such as the kidney, the proximal

Abbreviations

DW = diffusion weighted, FOV = field of view, PI-RADS = Prostate Imaging Reporting and Data System, PSA = prostate-specific antigen, PSMA = prostate-specific membrane antigen, SUV_{max} = maximum standardized uptake value, 3D = three-dimensional, 2D = two-dimensional

Summary

This pilot prospective study shows that preoperative whole-body gallium 68 prostate-specific membrane antigen–11 PET/MR imaging offers incremental value over dedicated prostate multiparametric MR imaging for preoperative prostate cancer localization and staging.

Implication for Patient Care

Gallium 68 prostate-specific membrane antigen 11 (or 68Ga-PSMA-11) is a promising PET radiopharmaceutical for localization of disease in patients with newly diagnosed intermediate- or high-risk prostate cancer.

small intestine, or the salivary glands (10). It provides a promising target for prostate cancer–specific imaging (11). Recently, methods have been developed to label PSMA ligands with gallium 68 (^{68}Ga) enabling their use for positron emission tomographic (PET) imaging and therapy (12). Initial experience with PET/CT using Glu-NH-CO-NH-Lys-(Ahx)-[^{68}Ga (HBED-CC)] (^{68}Ga-PSMA-11) as a ^{68}Ga-labeled PSMA ligand suggests that this tracer can reveal prostate cancer relapses and metastases with high contrast by binding to the extracellular domain of PSMA, followed by internalization (13). Increased detection of occult metastatic disease could improve treatment efficacy through better patient selection for treatments such as extended pelvic lymph node dissection or radiation for patients with evidence of nodal metastases outside the standard lymph node treatment area. Moreover, better localization of cancer within the prostate itself would also have a clinical impact by guiding image-targeted biopsy and patient selection for focal therapy.

PET/MR imaging is a hybrid technology that can provide both biologic and morphologic information about various biologic pathways. Compared with PET/CT, simultaneous PET/MR imaging has advantages resulting from reduced radiation exposure and higher soft-tissue contrast (14). PET/MR imaging is particularly important for accurate localization and assessing the pelvic extent of disease in the initial staging of prostate cancer. In fact, the majority of pathologic findings leading to upstaging are microscopic, requiring the high resolution of intraprostatic anatomy and adjacent structures afforded by coregistration with MR imaging rather than CT (15).

The purpose of this study was to report the results of dual-time-point ^{68}Ga-PSMA-11 PET/MR imaging prior to prostatectomy in patients with intermediate- or high-risk cancer.

Materials and Methods

Study Population

The Stanford Institutional Review Board and the Stanford Scientific Review Committee approved this prospective protocol conducted under IND #128379. Written informed consent was obtained. Inclusion criteria were as follows: *(a)* biopsy-proven intermediate- to high-risk prostate adenocarcinoma as determined by elevated PSA level (PSA > 10 ng/mL), T-stage (T2b or greater), or Gleason score (≥7); *(b)* scheduling for prostatectomy with pelvic lymph node dissection; *(c)* a Karnofsky performance status of greater than 50 (or the Eastern Cooperative Oncology Group/World Health Organization equivalent); and *(d)* availability of conventional imaging studies (CT, MR imaging, technetium-99m medronic acid bone scan), as indicated by clinical guidelines. Exclusion criteria were as follows: *(a)* exceeding the weight limit of the scanner, claustrophobia, or an inability to lie still for the duration of the examination; *(b)* neoadjuvant chemotherapy or radiation therapy prior to prostatectomy; *(c)* androgen deprivation therapy prior to PET imaging; and *(d)* metallic implants contraindicated for MR imaging. Forty-five men who were eligible for the study were recruited, and 35 consented. Examinations were cancelled for two of the enrolled patients because of claustrophobia in one instance and scanner malfunction in the other.

Preparation of ^{68}Ga-PSMA-11

We synthesized ^{68}Ga-PSMA-11 as previously reported (16). The precursor, Glu-NH-CO-NH-Lys (Ahx)-HBED-CC (DKFZ-PSMA-11, or PSMA-HBED), was obtained from ABX (Radeberg, Germany). All other reagents of the highest grade (eg, Sigma, EMD Millipore, Hospira, Akorn) were purchased from commercial suppliers and were used as provided. The radiosynthesis was performed with a fully automated synthesis device by using sterile single-use cassettes (Modular Laboratory PharmTracer; Eckert & Ziegler Eurotope, Berlin, Germany).

PET/MR Imaging Protocol

No specific patient preparation was required prior to the ^{68}Ga-PSMA-11 examinations. Imaging (vertex to midthighs) began at 41–61 minutes (mean, 0.2 minutes ± 5.4 [standard deviation]) after injection of a target fixed-dose of 185 MBq (5 mCi) (mean, 151.7 MBq ± 25.9; range: 108.8–184.6 MBq, 2.94–4.99 mCi) of ^{68}Ga-PSMA-11 by using a time-of-flight–enabled simultaneous PET/MR imaging unit (SIGNA PET/MR; GE Healthcare, Waukesha, Wis). The mean study duration was 76 minutes ± 14.2 (range, 28–95). The PET acquisition was performed in three-dimensional mode and for 4 minutes per bed position (89 sections per bed) in 5–9 beds. Additional delayed images of the prostate bed were acquired at 87–125 minutes (mean, 103.0 minutes ± 8.6) after injection. An axial two-point Dixon three-dimensional T1-weighted spoiled gradient-echo MR sequence (repetition time msec/echo time 1 msec/echo time 2 msec, 4.1/1.1/2.2; field of view [FOV] 50 × 37.5 cm; matrix, 256 × 128; section thickness/spacing: 5.2/2.6 mm; 120 images per slab; imaging time, 18 seconds) was acquired at each table position and used to generate attenuation correction maps and for anatomic registration of the PET results. PET images were reconstructed using ordered subset expectation maximization protocol with two iterations and 28 subsets. Time-of-flight reconstructed images assumed a Gaussian kernel of 400 ps width. The Dixon MR imaging sequence and the PET acquisition started at the same table po-

sition and times, thus ensuring optimal temporal and regional correspondence between MR imaging and PET data. For attenuation correction, the images were segmented into different tissue types with an anatomy-aware algorithm, and were coregistered to an MR imaging atlas in the head region (17). Additional sequences are described in Table E1 (online).

Additional sequences acquired at each station included the following: coronal T2-weighted single-shot fast spin echo (SSFSE), coronal diffusion weighted (DW), and T1-weighted axial two-point Dixon three-dimensional (3D) spoiled gradient echo. T2-weighted images were acquired by using a prototype SSFSE sequence with variable refocusing flip angles and outer volume suppression (18). SPECIAL (spectral inversion at lipids) fat suppression was applied at every other station. Because of the large prescribed FOV (FOV: 44 cm, phase FOV: 1), each acquisition covered two consecutive beds, allowing T2-weighted whole-body images with and without fat suppression to be retrospectively generated. Other imaging parameters for T2-weighted SSFSE were as follows: repetition time msec/echo time msec, 600–750/110; bandwidth, 105 kHz; matrix, 320 × 224; section thickness/skip, 8/2 mm; 28–38 sections; number of excitations, 0.75; ARC acceleration factor, 3; and imaging time, 25–30 seconds. Coronal DW imaging was performed using a custom-developed two-dimensional (2D) single-shot echo-planar imaging sequence, with 2D spatial selectivity obtained by replacing the conventional spectral-spatial excitation pulse with a 2D radiofrequency pulse (19). Imaging parameters were as follows: 2500/65; matrix size, 160 × 160; section thickness/skip, 8/0 mm; 32 sections; FOV: 44 cm; phase FOV: 0.55; half NEX with homodyne reconstruction; ASSET acceleration factor, two; b = 50 and 800 sec/mm^2 (eight and 16 NEX, respectively); and imaging time, 2:30 seconds. T1-weighted images were acquired by using an axial two-point Dixon 3D gradient-echo sequence (LAVA-flex; 4.9/1.3/2.5; flip angle, 15°; bandwidth, 142.86 kHz; FOV: 44 cm; matrix, 320 × 224; section thickness, 3.4 mm; ARC acceleration factor, 2 × 2; and imaging time, 0:21–0:55 minute). In the thorax region, the MR imaging acquisitions were performed during a breath hold in shallow inspiration, with the exception of DW imaging, which was always performed during free breathing. For the later acquisition over the prostate bed, the following sequences were included: small FOV axial T2 weighted, DW imaging, and coronal SSFSE with and without fat suppression.

Image Analysis

Two nuclear medicine physicians (A.I., with 13 years of experience and C.Z., with 5 years of experience) each reviewed the PET images using MIMvista, version 6.2 (MIMvista, Cleveland, Ohio) independently. PET images were reviewed in correlation with MR imaging images for identification of focal ^{68}Ga-PSMA-11 uptake within and outside the prostate, where a PET positive finding was defined as uptake higher than the surrounding background and not associated with physiologic uptake, considered suspicious for malignancy (20). Maximized standardized uptake values (SUV_{max}) for both early and delayed images were recorded by a third reader (S.P., 7 years experience) for all detected lesions. The MR imaging images (multiparametric, including DW imaging, T2-weighted imaging and DCE covering the prostate) were analyzed preoperatively, blinded to the PET/MR imaging results by radiologists specializing in body MR imaging (P.G., 7 years experience; A.L., 4 years experience) who used the PI-RADS version 2 criteria (21). The readers were blinded to clinical and pathologic data, except for the knowledge of diagnosis of biopsy-proven prostate cancer. The mean time intervals from biopsy to PET and MR imaging were 9.1 weeks ± 5.5 (standard deviation) (range, 1–30 weeks) and 4 weeks ± 3.8 (range, 1–15), respectively.

Histopathologic Correlation

While undergoing multiparametric MR imaging -ultrasound fusion targeted prostate biopsy, the prostate gland was segmented on T2-weighted images using Profuse (Eigen, Grass Valley, Calif). This was used to create a three-dimensional (3D) volume which was then imported into modeling software (SketchUp, Trimble, Sunnyvale, Calif or SolidWorks, Dassault, France) to create a custom, personalized mold, such that the orientation of an ex vivo prostate could be held in the same plane as the original MR imaging acquisition. Channels were created so that gross sections were 3.5 mm thick to match the resolution of the T2-weighted images as well. Following radical prostatectomy, these 3D-printed, patient-specific molds were used to guide the gross sectioning of the ex vivo prostate. After fixation and staining, these sections were mounted onto slides, and a digital slide scanner such as the NanoZoomer (Hamamatsu, Japan) was used to render high quality images and high resolution for side-by-side comparisons between the preprocedure imaging and final pathology. Hematoxylin-eosin–stained slides from whole mount prostatectomies were scanned using an Aperio CS2 (Leica Biosystems, Wetzlar, Germany). These were then annotated by a pathologist to outline areas of cancer as well as the borders of the gland using Imagescope software v.12.3.2.8013 (Leica Biosystems). Using the same software, the areas of the annotated regions were measured and percent of gland involved was calculated from these values. Postoperative PSA and clinical follow-up were reviewed.

Statistical Analysis

Sensitivity and specificity were calculated for ^{68}Ga-PSMA-11 PET and multiparametric MR imaging on a per-patient and per-lobe basis for the primary tumor and per-node against the gold standard of surgical histopathology. Early and delayed SUV_{max} were compared by using a paired t test. After testing the assumption of normality with the Kolmogorov-Smirnov test, the two metabolic parameters were correlated with PSA by using the Pearson correlation, and with Gleason score and tumor volume by using the Spearman correlation. Further subgroup analysis was done according to PI-RADS score and lymph node status. All statistical analyses were performed by using SPSS Statistics, version 22 (IBM, Armonk, NY). $P < .05$ was considered to indicate a significant difference.

Results

Thirty-three men (mean age, 66.5 years ± 3.9; range, 55–74 years) scheduled for prostatectomy and matching study criteria

Table 1: Characteristics of 33 Patients

Characteristic	Finding
Age (y)*	66.4 ± 4.0 (55–74)
PSA level (ng/mL)*	9.6 ± 5.8 (3.7–34.5)
Gleason score	
7	18 (55)
8	8 (24)
9	7 (21)
Clinical stage	
T1c	15 (45)
T2a	5 (15)
T2b	7 (21)
T2c	4 (12)
T3a	2 (6)
Risk according to D'Amico classification	
Intermediate	18 (55)
High	15 (45)

Note.—Unless otherwise specified, data are numbers of patients, with percentages in parentheses. PSA = prostate-specific antigen.
* Data are means ± standard deviations, with ranges in parentheses.

were prospectively enrolled; 18 had intermediate-risk and 15 had high-risk prostate cancer according to the D'Amico classification (22). Detailed demographics are shown in Table 1. Scans were performed between April 2016 and September 2017, with a mean clinical follow-up of 8.7 months (SD: 5.7 months, range: 1–20).

The results of conventional imaging and the time between them and PET/MR imaging are shown in Table 2. The time from biopsy diagnosing prostate cancer to ^{68}Ga-PSMA-11 PET/MR imaging ranged from 1 to 30 weeks (mean, 9.1 weeks ± 5.5). The time from ^{68}Ga-PSMA-11 PET/MR imaging to prostatectomy ranged from 1 to 9 weeks (mean, 1.8 ± 1.8). The variability is due to the length of time it took participants to decide to undergo surgery (including scheduled visit with surgeon after biopsy and obtaining insurance authorization for the procedure), since scheduled prostatectomy was required as part of inclusion criteria. There was no treatment between the scans and prior to surgery.

Two independent PET readers identified abnormal tracer uptake in the prostate of all patients with 100% agreement. These areas always overlapped the tumor regions determined by whole-mount surgical pathology (Fig 1), except for one high-risk patient (PSA 5.5, Gleason score 4+4, cT1c) in whom involvement appeared to be bilateral but was confined to a single lobe on final pathology, yielding an 84.8% sensitivity and 87.5% specificity on a per-lobe basis. A more diffuse pattern of uptake was seen in three patients, for which the precise number of lesions could not be determined. According to histopathologic evaluation, all three were Gleason score 7; two had bilateral involvement and one had 60% tumor involvement. The latter patient also demonstrated focal uptake in the vas deferens, and histopathologic examination confirmed seminal vesicle invasion (Fig 2).

Meanwhile, multiparametric MR imaging identified PI-RADS 4 and 5 lesions in 26 (78.8%) of 33 patients and PI-RADS 3 lesions in four (Table 3). The sensitivity and specificity for PI-RADS 4 or 5 on a per-lobe basis were 52.5% and 100%, respectively (Table 4) The seven patients with PI-RADS 3 or lower showed no differences in terms of Gleason score or preoperative PSA, but had a smaller tumor volume (mean 9.6% involvement compared with 19.8% in PI-RADS 4 or 5, $P = .018$). All three patients with a tumor volume < 5% had a PI-RADS score of 3 or lower. Of the three tumors not identified with multiparametric MR imaging, the PI-RADS 2 patient was intermediate risk (PSA 9.9, Gleason score 3+4, cT1c) with < 5% tumor involvement on final pathology. The two PI-RADS 1 patients were high risk (PSA 11.6, Gleason score 4+4, cT1c and PSA 14.3, Gleason score 4+5, cT1c) with 40% and < 5% tumor involvement on final pathology, respectively. Both had extracapsular extension and the latter also demonstrated seminal vesicle invasion. SUVs of the prostate regions of interest from the delayed PET images of the pelvis were significantly higher than those from the earlier whole-body images (mean: 15.3 vs 12.3, $P < .001$) (Table 5), although there were a few individual lesions that decreased in SUV over time. In three cases, conflicting temporal trends of uptake were found in different foci of the same patient. PSA correlated with tumor volume ($\rho = 0.445$, $P = .011$) and SUV_{max} at both time points ($r = 0.491$, $P = .004$ and $r = 0.518$, $P = .003$, respectively), while Gleason score did not show any significant relationship. Tumor volume correlated with initial SUV_{max} ($\rho = 0.444$, $P = .011$), but not delayed SUV_{max} ($\rho = 0.348$, $P = .055$). The delayed images showed only one additional lesion, which was ultimately proven on pathology to be cancer, in the prostate of a patient with bilateral involvement (Fig 3). Both multiparametric MR imaging and the earlier PET images identified the focus in the left lobe, but the focus in the right lobe was only seen on delayed images, yielding an 86.4% sensitivity and 87.5% specificity on a per-lobe basis. Another interesting patient demonstrated no abnormality on multiparametric MR imaging (PI-RADS 1), but a single focus was suspected on the earlier PET images which later became considerably more discrete. Notably, the SUVmax for the two time-points remained the same (both 4.3), but with decreased background activity in the delayed imaging.

The pelvic nodal dissection resulted in removal of 183 (mean ± SD: 5.5 ± 3.6, range, 1–17 per patient) left pelvic lymph nodes and 199 (6.0 ± 3.8, range 1–20 per patient) right pelvic lymph nodes. Postoperative PSA values dropped to <0.5 ng/mL for all but one patient. Twelve of these were confirmed at histopathologic examination to harbor metastatic disease in three patients, all of whom had PET-positive pelvic lymph nodes that were not identified on multiparametric MR imaging. Twelve abnormal pelvic lymph nodes were noted on PET in five patients, half of which were confirmed as metastatic at surgical pathologic examination. True-positive nodes had higher SUVs than false-positive nodes (mean initial SUV_{max} 6.9 vs 2.2, $P = .021$; mean delayed SUV_{max} 7.5 vs 1.9, $P = .005$). Notably, one patient showed intense ^{68}Ga-PSMA-11 PET uptake in the sternum, confirming the bone metastasis that was suspected on the bone scan but not included in the FOV of other cross-sectional imaging.

Table 2: Results of Conventional Imaging Performed prior to ^{68}Ga-PSMA-11 PET/MR Imaging for Metastasis

	MR Imaging of Pelvis		CT of Abdomen and Pelvis		^{99m}Tc MDP Bone Scanning	
Patient No.	Finding	Time to PET/MR Imaging (wk)	Finding	Time to PET/MR Imaging (wk)	Finding	Time to PET/MR Imaging (wk)
1	Negative	1	Negative	5	Negative	5
2	B/L external iliac lymph nodes	34	Negative	25	Negative	22
3	Negative	1	Negative	12	Negative (trauma in right 6–7th ribs)	7
4	Negative	7	NA	NA	Negative	4
5	Negative	7	B/L iliac lymph nodes	9	Negative (trauma in left mid tibia)	9
6	Negative	9	NA	NA	Negative	11
7	Negative	10	NA	NA	Negative	7
8	Negative	16	NA	NA	Negative	11
9	Negative	1	Negative	38	Negative	38
10	Negative	10	NA	NA	Negative	2
11	Negative	9	NA	NA	NA	NA
12	Negative	8	NA	NA	Negative	4
13	Negative	15	NA	NA	NA	NA
14	Negative	15	Negative	5	NA	NA
15	Negative	10	NA	NA	NA	NA
16	Negative	12	Negative	19	NA	NA
17	Right external iliac lymph node	17	NA	NA	NA	NA
18	Negative	13	NA	NA	Negative	10
19	Negative	30	NA	NA	Negative	9
20	Negative	1	Negative	7	Negative (trauma in right 9th rib)	8
21	Negative	1	Negative	16	Negative	16
22	Negative	23	NA	NA	Negative	3
23	Negative	4	NA	NA	Negative	8
24	Negative	1	Negative	3	NA	NA
25	B/L inguinal and external iliac lymph nodes	13	B/L inguinal and external/internal iliac lymph nodes	3	Negative	1
26	Negative	8	Negative	11	Negative	11
27	Negative	4	NA	NA	NA	NA
28	Pelvic lymph node	1	Negative	3	Negative (trauma in sternum and ribs)	3
29	Negative	11	Negative	2	Negative	2
30	Pelvic lymph node	1	Negative	6	Negative	3
31	Negative	13	Negative	1	Negative	4
32	Negative	12	Negative	4	Negative	9
33	Negative	13	Negative	1	Negative	6

Note.—B/L = bilateral, MDP = methylene diphosphonate, NA = not available, ^{99m}Tc = technetium 99m.

Discussion

This prospective pilot study evaluates the role of dual-time-point ^{68}Ga-PSMA-11 PET/MR imaging in the detection of cancer within the prostate and pelvic lymph nodes for initial staging of patients with intermediate or high-risk prostate cancer, by direct correlation with whole-mount pathology from radical prostatectomy and pelvic lymph node dissection. While the clinical value of ^{68}Ga-PSMA-11 PET in men with biochemically persistent or recurrent prostate cancer is widely documented (23–25), its role in the assessment of primary prostate cancer remains a topic of continued investigation. The few previous retrospective studies using ^{68}Ga-PSMA-11 for initial staging reported a 90.5%–95.8% accuracy on a per-patient basis, in which at least one prostate cancer-associated lesion was detected (26–30).

Table 3: Results of Image Interpretation and Histopathologic Examination, with PSA Level Follow-up (When Available)

Patient No.	Biopsy to PET/MRI (wk)	^{68}Ga-PSMA-11 PET		Multiparametric MR Imaging (PI-RADS Category)	PET/MR Imaging to Surgery (wk)	Histopathologic Findings			PSA Level (ng/mL)		Follow-up (mo)
		Prostate	LNs			Prostate GS and TV (%)	Left LNs	Right LNs	Before Surgery	After Surgery	
1	1	Right	Negative	Right (4)	1	Bilateral (4+3, 20%)	Negative (0/4)	Negative (0/10)	9.70	<0.01	20
2	30	Diffuse	Negative	Right (5)	1	Right (4+4, 5%)	Negative (0/7)	Negative (0/7)	5.50	<0.05	19
3	11	Diffuse	Negative	Bilateral two foci (4,5)	1	Bilateral (3+4, 60%)	Negative (0/2)	Negative (0/3)	15.00	NA	1
4	4	Bilateral four foci	Negative	Right (5)	4	Bilateral (4+4, 10%)	Negative (0/10)	Negative (0/7)	4.12	<0.03	16
5	10	Bilateral three foci	Negative	Right (5)	1	Bilateral (3+4, 5%)	Negative (0/2)	Negative (0/4)	8.50	<0.05	12
6	15	Bilateral three foci	Negative	Left (5)	5	Bilateral (4+5, 15%)	Negative (0/5)	Negative (0/3)	16.00	<0.02	6
7	9	Left	Positive, one (left)	Left (5), central apical (5)	6	Bilateral (4+5, 50%)	Positive (1/9)	Negative (0/5)	10.40	<0.02	15
8	14	Bilateral two foci	Negative	Bilateral three foci (4)	1	Bilateral (4+3, 30%)	Negative (0/7)	Negative (0/5)	34.50	<0.016	12
9	13	Bilateral two foci	Negative	Bilateral two foci (3)	4	Bilateral (3+4, 5%)	Negative (0/5)	Negative (0/7)	6.70	<0.05	11
10	9	Diffuse	Negative	Bilateral two foci (3)	2	Bilateral (3+4, 10%)	Negative (0/9)	Negative (0/1)	11.30	0.05	14
11	7	Bilateral three foci	Positive, one (left)	Right two foci (2)	1	Bilateral (3+4, < 5%)	Negative (0/13)	Negative (0/7)	9.90	<0.05	14
12	3	Left	Negative	Left (5)	1	Left (4+4, 10%)	Negative (0/3)	Negative (0/11)	6.81	<0.02	13
13	9	Left	Negative	Left (5)	1	Left (4+3, 30%)	Negative (0/10)	Negative (0/4)	7.57	<0.05	12
14	14	Right	Negative	Right (4)	1	Right (4+3, 10%)	Negative (0/6)	Negative (0/6)	5.20	0.02	12
15	9	Bilateral three foci	Negative	Right two foci (4)	3	Bilateral (3+4, 10%)	Negative (0/7)	Negative (0/8)	3.70	<0.02	12
16	8	Bilateral three foci	Negative	Left (4)	1	Bilateral (4+3, 15%)	Negative (0/5)	Negative (0/4)	4.58	NA	1
17	14	Left two foci	Negative	Left (5)	1	Left (4+3, 20%)	Negative (0/1)	Negative (0/4)	6.00	<0.05	9
18	13	Right	Negative	No lesion (1)	1	Right (4+4, 40%)	Negative (0/7)	Negative (0/10)	11.60	<0.02	7
19	15	Right	Negative	Right (4)	9	Bilateral (4+4, 20%)	Negative (0/4)	Negative (0/4)	10.30	<0.0008	6
20	6	Left	Negative	Left (4)	1	Bilateral (4+3, 30%)	Negative (0/1)	Negative (0/1)	16.20	<0.1	10
21	14	Bilateral three foci	Positive, one (left)	Right two foci (4,5)	1	Bilateral (4+5, 40%)	Positive (3/17)	Positive (4/20)	15.20	<0.1	2
22	10	Bilateral two foci	Positive, one (right)	Right (4)	1	Bilateral (4+4, 5%)	Negative (0/6)	Negative (0/6)	6.30	<0.05	9

Table 3 *(continues)*

Table 3 *(continued)*: Results of Image Interpretation and Histopathologic Examination, with PSA Level Follow-up (When Available)

Patient No.	Biopsy to PET/MRI (wk)	^{68}Ga-PSMA-11 PET		Multiparametric MR Imaging (PI-RADS Category)	PET/MR Imaging to Surgery (wk)	Histopathologic Findings			PSA Level (ng/mL)		Follow-up (mo)
		Prostate	LNs			Prostate GS and TV (%)	Left LNs	Right LNs	Before Surgery	After Surgery	
23	3	Bilateral two foci	Positive, three (bilateral)	Right (3)	1	Bilateral (4+5, < 5%)	Negative (0/6)	Negative (0/7)	4.90	<0.05	0
24	3	Bilateral two foci	Negative	Left two foci (4)	1	Bilateral (4+3, 10%)	Negative (0/2)	Negative (0/5)	5.66	<0.05	8
25	7	Bilateral two foci	Negative	Right (3)	1	Bilateral (3+4, 5%)	Negative (0/3)	Negative (0/8)	5.10	<0.05	9
26	7	Right	Positive, four (bilateral)	Right (4)	1	Bilateral (4+3, 10%)	Negative (0/5)	Positive (4/11)	13.20	<0.05	8
27	2	Left	Negative	Left (5)	1	Bilateral (3+4, 10%)	Negative (0/4)	Negative (0/1)	5.20	<0.05	5
28	4	Bilateral multifocal	Negative	Left (5)	1	Bilateral (4+5, 40%)	Negative (0/1)	Negative (0/4)	9.39	<0.1	8
29	7	Bilateral multifocal	Positive, one (left)	Bilateral three foci (4)	1	Bilateral (3+4, 5%)	Negative (0/4)	Negative (0/2)	8.70	NA	1
30	4	Right	Negative	Right (5)	1	Bilateral (4+4, 10%)	Negative (0/2)	Negative (0/6)	10.69	NA	2
31	6	Bilateral three foci	Negative	Left (4)	1	Bilateral (4+4, 5%)	Negative (0/8)	Negative (0/6)	8.70	<0.02	6
32	11	Bilateral two foci	Negative	No lesion (1)	1	Bilateral (4+5, < 5%)	Negative (0/6)	Negative (0/11)	14.30	0.26	5
33	8	Right	Negative	Right (4)	1	Bilateral (4+5, 5%)	Negative (0/3)	Negative (0/5)	4.30	<0.1	4

Note.—GS = Gleason score, LN = lymph node, NA = not available (lost to follow-up), PI-RADS = Prostate Imaging Reporting and Data System, PSA = prostate-specific antigen, PSMA = prostate-specific membrane antigen, ^{68}Ga = gallium 68, TV = total volume.

Table 4: Diagnostic Accuracy of PET and multiparametric MR imaging

	"Positive" Examination		"Negative" Examination		Diagnostic Accuracy (%)	
Modality and Analysis	True-Positive	False-Positive	True-Negative	False-Negative	Sensitivity	Specificity
Reference standard PET						
Per patient	33	0	0	0	100	
Per lobe	50	1	9	7	86.4	87.5
Per node	6	6	366	6	50	98.4
Multiparametric MR imaging						
Per patient	26	0	0	7	79.4	
Per lobe	31	1	28	7	52.5	100
Per node	0	9	367	12	0	97.6

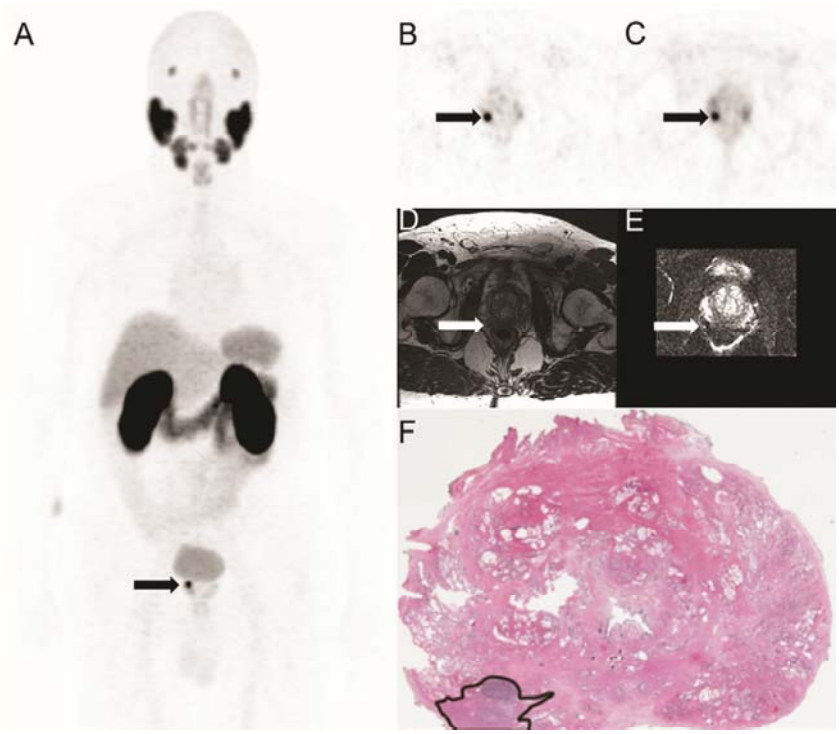

Figure 1: Images in 74-year-old man (patient 4) with recently diagnosed intermediate-risk T1c Gleason 4+4 prostate cancer (arrows) with a prostate-specific antigen level of 4.12 ng/mL. *A*, Maximum intensity projection PET image, *B*, early transaxial PET image, and, *C* delayed transaxial PET image show focal uptake in, *F*, histopathologically proven prostate cancer (hematoxylin-eosin stain; original magnification, ×1.25). The milder focal uptake in the left lobe was likewise proven to be prostate cancer. *D*, Transaxial T2-weighted MR image and, *E*, diffusion-weighted (b = 800 sec/mm^2) MR image are also shown. Only the right-side tumor was positive at multiparametric MR imaging (Prostate Imaging Reporting and Data System category 5).

In both studies that included comparisons between the modalities, ^{68}Ga-PSMA-11 PET outperformed multiparametric MR imaging (28,29). All 33 of our patients were overall PET-positive for detection of prostate cancer, while multiparametric MR imaging identified high likelihood of clinically important cancer (PI-RADS 4–5) in 79%, which is in keeping with the 48%–78% sensitivity in the literature (31–34). Both PI-RADS score and SUV_{max} correlated with tumor volume in our study, while subanalysis showed that patients with PI-RADS 3 or lower had a smaller tumor volume, suggesting that the difference in sensitivity may be due in part to better visualization of small prostate lesions.

In addition to intraprostatic tumor localization, accurate detection of local-regional lymph node metastases may play an important role, especially when deciding the need for radiation to the pelvic lymph nodes or the extent of pelvic node dissection at prostatectomy. A recent study by Obek et al (35) reported a PET sensitivity in detecting lymph node metastasis of 53%–67%, compared with 25% by morphologic imaging. Although there is only preliminary data, ^{68}Ga-PSMA-11 imaging (36) appears to outperform MR imaging (37), which relies on abnormal anatomic characteristics (eg, non-oval shape, short-axis diameter > 1 cm) for identification of pathologic lymph nodes (38). In our cohort, ^{68}Ga-PSMA-11 PET demonstrated a 50% sensitivity per node, while multiparametric MR imaging was unable to correctly identify any of the metastatic lymph nodes. Also importantly, all patients with normal pelvic nodes in PET were negative for metastases at pathologic examination. This is promising in that a high negative predictive value of ^{68}Ga-PSMA-11 PET would allow more informed clinical decision-making regarding the need for pelvic nodal dissection; however, this requires a larger cohort for further evaluation.

While PET may provide improved specificity, MR imaging offers high spatial resolution leading to higher accuracy in delineating tumor location (39). As PET/MR imaging hybrid scanners become increasingly available, there is an opportunity to improve imaging for primary tumors by coregistering the higher resolution and anatomic landmark definition derived from MR imaging with the improved intraprostatic specificity and molecular information for N and M staging by PET. In the only other ^{68}Ga-PSMA-11 PET/MR imaging comparison study for primary prostate cancer validated by histopathology, Eiber

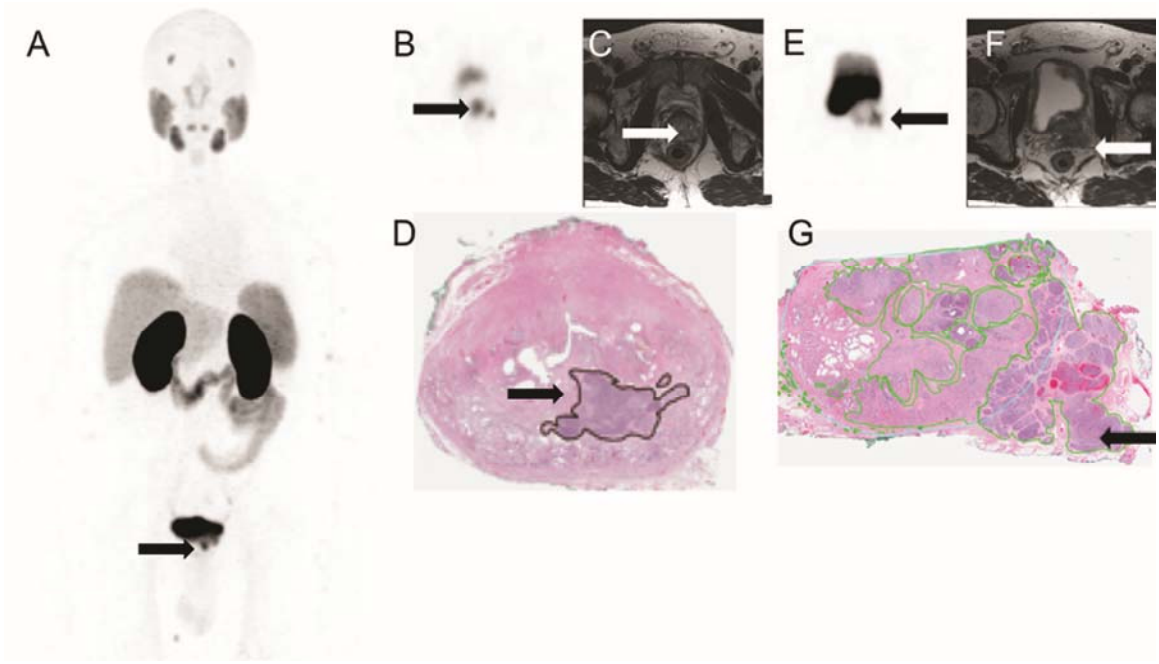

Figure 2: Images in 66-year-old man (patient 7) with recently diagnosed high-risk T2b Gleason 4+5 prostate cancer (arrows) with a prostate-specific antigen level of 10.40 ng/mL. *A,* Maximum intensity projection PET image and, *B,* early transaxial PET image show focal uptake in, *D,* histopathologically proven prostate cancer (hematoxylin-eosin stain; original magnification, ×1.25), which was classified as Prostate Imaging Reporting and Data System category 5 at MR imaging. *C,* Transaxial T2-weighted MR image is also shown. *E,* Early transaxial PET image showed focal uptake in, *G,* histopathologically proven involvement of left vas deferens. This involvement was also noted at multiparametric MR imaging. *F,* Transaxial T2-weighted MR image is also shown.

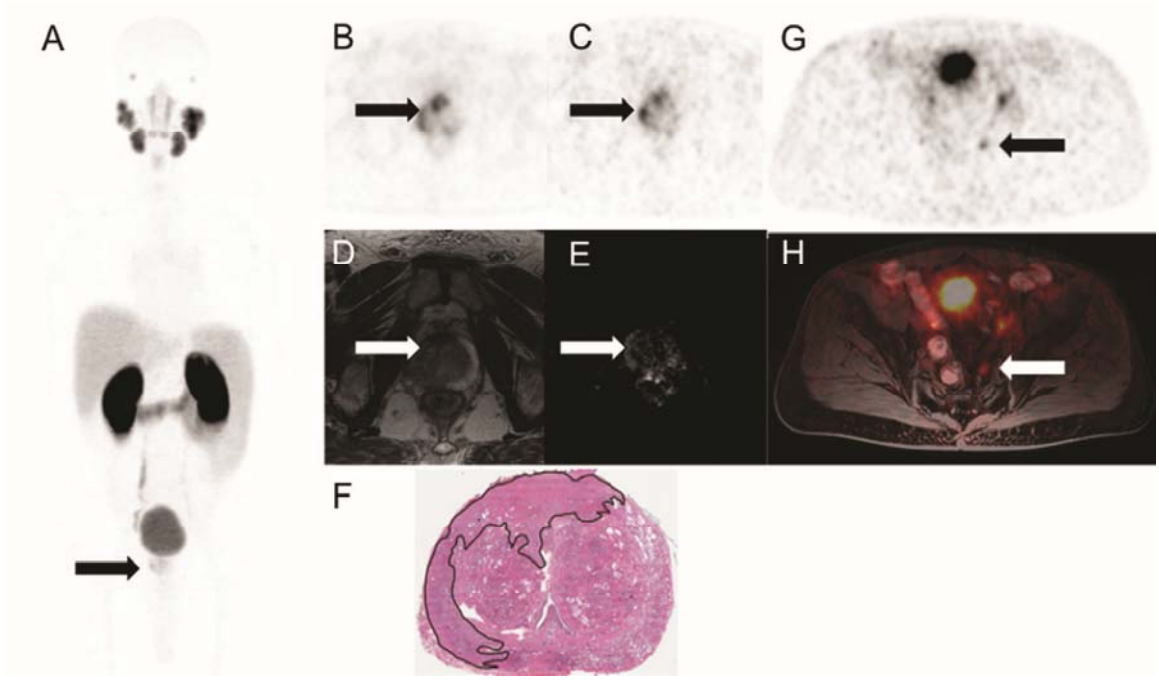

Figure 3: Images in 65-year-old man (patient 21) with recently diagnosed high-risk T2b Gleason 4+5 prostate cancer and a PSA of 15.20 ng/mL. *A,* Maximum intensity projection PET image, *B,* early transaxial PET image, and, *C,* delayed transaxial PET image show focal uptake (arrows) in, *F,* histopathologically proven prostate cancer (hematoxylin-eosin stain; original magnification, ×1.25), which was classified as Prostate Imaging Reporting and Data System category 5 at MR imaging. *D,* Transaxial T2-weighted MR image and, *E,* diffusion-weighted (b = 1200 sec/mm^2) MR image are also shown (arrows = lesion). *G,* Early transaxial PET image and, *H,* transaxial T1-weighted fused PET/MR image show focal uptake in left pelvic lymph node (black arrow in *G*; white arrow in *H*) that had not been noted at multiparametric MR imaging. The area of the lymph node was not included in the delayed field of view.

Table 5: Semiquantitative Analysis of Dual-Time-Point Imaging

Parameter	PSMA Dose (mCi)*	Early Imaging (min PI)	Delayed Imaging (min PI)	Early SUV_{max}	Delayed SUV_{max}
Mean ± standard deviation	4.1 ± 0.7	50.1 ± 5.3	103.0 ± 8.6	12.3 ± 8.9	15.3 ± 11.9
Range	2.9–5.0	41–61	87–125	3.6–34.5	4.1–50.7

Note.—PI = postinjection, PSMA = prostate-specific membrane antigen, SUV_{max} = maximum standardized uptake value.
* To convert to Système International units (megabequerels), multiply by 37.

et al (29) reported that the diagnostic accuracy of simultaneous PET/MR imaging outperformed both multiparametric MR imaging and PET imaging alone. Notably, each of the latter two methods was able to identify tumor-involved areas that were negative in the other modality, leading to superior sensitivity of PET/MR imaging on a per-patient basis as well as by sextant.

The intensity of ^{68}Ga-PSMA-11 accumulation can be predicted by PSA and Gleason score (40). We confirmed that SUV_{max} correlated significantly with PSA and also found that both SUV_{max} and PSA correlated with tumor volume. Meanwhile, a recent immunohistochemical validation study by Woythal et al (41) reported conflicting results, with no correlation between SUV_{max} and tumor size, although the metabolic parameter did indeed correlate with immunoreactive score as well as percentage of stained cells. One possible explanation for this inconsistency is that the prognostic value of tumor volume has been shown to be stronger when expressed as a percentage of the prostate occupied by the tumor, as in our study, compared with size measurements especially given that the prostate size is in and of itself another important predictive variable (42). Notably, both our study and Woythal et al found no correlation between SUV_{max} and Gleason score, which may point to the inherent bias of the limited range of Gleason scores included in both studies.

To our knowledge, there have been four publications regarding multiple time-point ^{68}Ga-PSMA-11 imaging (26,30,43,44). Schmuck et al (26) found that the primary prostate tumor could be identified in 19 (95%) of 20 patients on the early dynamic images, as well as static scans after 60 minutes and 180 minutes postinjection. More recently, the group reported limited impact of delayed imaging, with improved contrast but no difference in actual detection rates between the two static time points (44). Similarly, our detection rates remained the same for both time-points on a per-patient basis, although an additional cancer focus was found. Afshar-Oromieh et al (43) reported higher detection rates and lesion visibility at 3 hours after injection compared with 1 hour, but these PET-positive lesions were not evaluated for confirmation with histopathology as a reference standard. Further studies are warranted to determine the clinical impact of such additional imaging.

Our results also showed that tracer accumulation increased overall at later acquisition times, including the metastatic uptake in the vas deferens (SUV_{max}, 23.9–32.5). Again, a minority of lesions demonstrated lower or stable SUVs. While the reasons for such decreased uptake remain unclear, it has been suggested that some lesions may show reduced internalization rate (43). This would present a challenge regarding potential efficacy in the development of promising anti-PSMA therapies such as ^{177}Lu-PSMA-617 (45) and ^{131}I-MIP-1095 (46).

A few limitations of our study must be noted. By design, patients in our cohort had intermediate- to high-risk prostate cancer and were therefore more likely to overexpress PSMA, possibly imparting higher accuracy (40,47). The accuracy of PET/MR imaging for low-risk cancer requires further evaluation. Another inherent limitation is the possibility that not all metastatic lymph nodes were removed. However, postoperative PSA values dropped to < 0.5 ng/mL in 32 patients, suggesting that this was not likely the case. Further follow-up of the postprostatectomy clinical course, especially regarding local tumor recurrence, would be of added interest.

In conclusion, this pilot prospective study shows that preoperative whole body ^{68}Ga-PSMA-11 PET/MR imaging offers incremental value over a dedicated prostate multiparametric MR imaging for preoperative cancer localization and staging. The high soft-tissue contrast of MR imaging enabled detailed localization of the radiotracer uptake within the prostate. Larger studies are needed to confirm if a negative ^{68}Ga-PSMA-11 PET/MR imaging for nodal metastases may eliminate the need for pelvic nodal dissection.

Acknowledgments: We thank our research coordinators Omar Rutledge, MS, and Jordan Cisneros, BS, the Cyclotron and Radiochemistry Facility, and the PET/MR imaging technologists. Special thanks to all the patients who agreed to participate in the study and their families.

Author contributions: Guarantors of integrity of entire study, S.Y.P., A.I.; study concepts/study design or data acquisition or data analysis/interpretation, all authors; manuscript drafting or manuscript revision for important intellectual content, all authors; manuscript final version approval, all authors; agrees to ensure any questions related to the work are appropriately resolved, all authors; literature research, S.Y.P., C.Z., C.H., F.G., P.G., B.D., A.I.; clinical studies, S.Y.P., C.H., N.H., F.G., P.G., B.D., A.M.L., G.A.S., A.I.; experimental studies, S.Y.P., C.H., R.E.F., C.K.; statistical analysis, S.Y.P., C.H., F.G.; and manuscript editing, S.Y.P., C.Z., C.H., F.G., P.G., B.D., A.M.L., G.A.S., A.I.

Disclosures of Conflicts of Interest: **S.Y.P.** disclosed no relevant relationships. **C.Z.** disclosed no relevant relationships. **C.H.** disclosed no relevant relationships. **R.E.F.** disclosed no relevant relationships. **C.K.** disclosed no relevant relationships. **N.H.** disclosed no relevant relationships. **F.G.** disclosed no relevant relationships. **P.G.** disclosed no relevant relationships. **B.D.** Activities related to the present article: institution received grant from GE Healthcare. Activities not related to the present article: disclosed no relevant relationships. Other relationships: disclosed no relevant relationships. **A.M.L.** Activities related to the present article: institution received grant from GE Healthcare. Activities not related to the present article: disclosed no relevant relationships. Other relationships: disclosed no relevant relationships. **G.A.S.** disclosed no relevant relationships. **A.I.** Activities related to the present article: institution received research support from GE Healthcare. Activities not related to the present article: disclosed no relevant relationships. Other relationships: disclosed no relevant relationships.

References

1. Siegel RL, Miller KD, Jemal A. Cancer statistics, 2017. CA Cancer J Clin 2017;67(1):7–30.

2. Smith RA, Cokkinides V, Brawley OW. Cancer screening in the United States, 2009: a review of current American Cancer Society guidelines and issues in cancer screening. CA Cancer J Clin 2009;59(1):27–41.
3. Lacy GL 2nd, Soderdahl DW, Hernandez J. Optimal cost-effective staging evaluations in prostate cancer. Curr Urol Rep 2007;8(3):190–196.
4. Roscigno M, Sangalli M, Mazzoccoli B, Scattoni V, Da Pozzo L, Rigatti P. Medical therapy of prostate cancer. A review. Minerva Urol Nefrol 2005;57(2):71–84.
5. Oh WK, Kantoff PW. Treatment of locally advanced prostate cancer: is chemotherapy the next step? J Clin Oncol 1999;17(11):3664–3675.
6. Jani AB. Management strategies for locally advanced prostate cancer. Drugs Aging 2006;23(2):119–129.
7. Puech P, Rouvière O, Renard-Penna R, et al. Prostate cancer diagnosis: multiparametric MR-targeted biopsy with cognitive and transrectal US-MR fusion guidance versus systematic biopsy--prospective multicenter study. Radiology 2013;268(2):461–469.
8. NCCN Clinical Practice Guidelines in Oncology. Prostate Cancer Version 2.2017. https://www.nccn.org/professionals/physician_gls/pdf/prostate.pdf. Published February 21, 2017. Accessed April 7, 2017.
9. Khan MA, Partin AW. Management of high-risk populations with locally advanced prostate cancer. Oncologist 2003;8(3):259–269.
10. Sweat SD, Pacelli A, Murphy GP, Bostwick DG. Prostate-specific membrane antigen expression is greatest in prostate adenocarcinoma and lymph node metastases. Urology 1998;52(4):637–640.
11. Eder M, Eisenhut M, Babich J, Haberkorn U. PSMA as a target for radiolabelled small molecules. Eur J Nucl Med Mol Imaging 2013;40(6):819–823.
12. Hillier SM, Maresca KP, Femia FJ, et al. Preclinical evaluation of novel glutamate-urea-lysine analogues that target prostate-specific membrane antigen as molecular imaging pharmaceuticals for prostate cancer. Cancer Res 2009;69(17):6932–6940.
13. Afshar-Oromieh A, Malcher A, Eder M, et al. PET imaging with a [68Ga] gallium-labelled PSMA ligand for the diagnosis of prostate cancer: biodistribution in humans and first evaluation of tumour lesions. Eur J Nucl Med Mol Imaging 2013;40(4):486–495.
14. Antoch G, Bockisch A. Combined PET/MRI: a new dimension in whole-body oncology imaging? Eur J Nucl Med Mol Imaging 2009;36(Suppl 1):S113–S120.
15. Engeler CE, Wasserman NF, Zhang G. Preoperative assessment of prostatic carcinoma by computerized tomography: weaknesses and new perspectives. Urology 1992;40(4):346–350.
16. Eder M, Neels O, Müller M, et al. Novel preclinical and radiopharmaceutical aspects of [68Ga]Ga-PSMA-HBED-CC: a new PET tracer for imaging of prostate cancer. Pharmaceuticals (Basel) 2014;7(7):779–796.
17. Iagaru A, Mittra E, Minamimoto R, et al. Simultaneous whole-body time-of-flight 18F-FDG PET/MRI: a pilot study comparing SUVmax with PET/CT and assessment of MR image quality. Clin Nucl Med 2015;40(1):1–8.
18. Loening AM, Saranathan M, Ruangwattanapaisarn N, Litwiller DV, Shimakawa A, Vasanawala SS. Increased speed and image quality in single-shot fast spin echo imaging via variable refocusing flip angles. J Magn Reson Imaging 2015;42(6):1747–1758.
19. Fung MM, Estkowski L, Xu D, et al. Coronal whole body diffusion imaging with 2D spatially selective excitation (FOCUS) [abstr]. In: Proceedings of the Twenty-Second Meeting of the International Society for Magnetic Resonance in Medicine. Berkeley, Calif: International Society for Magnetic Resonance in Medicine, 2014.
20. Rauscher I, Maurer T, Fendler WP, Sommer WH, Schwaiger M, Eiber M. (68)Ga-PSMA ligand PET/CT in patients with prostate cancer: how we review and report. Cancer Imaging 2016;16(1):14.
21. Weinreb JC, Barentsz JO, Choyke PL, et al. PI-RADS Prostate Imaging - Reporting and Data System: 2015, Version 2. Eur Urol 2016;69(1):16–40.
22. D'Amico AV, Whittington R, Malkowicz SB, et al. A multivariable analysis of clinical factors predicting for pathological features associated with local failure after radical prostatectomy for prostate cancer. Int J Radiat Oncol Biol Phys 1994;30(2):293–302.
23. Afshar-Oromieh A, Avtzi E, Giesel FL, et al. The diagnostic value of PET/CT imaging with the (68)Ga-labelled PSMA ligand HBED-CC in the diagnosis of recurrent prostate cancer. Eur J Nucl Med Mol Imaging 2015;42(2):197–209.
24. Eiber M, Maurer T, Souvatzoglou M, et al. Evaluation of hybrid ^{68}Ga-PSMA ligand PET/CT in 248 patients with biochemical recurrence after radical prostatectomy. J Nucl Med 2015;56(5):668–674.
25. Rauscher I, Maurer T, Beer AJ, et al. Value of 68Ga-PSMA HBED-CC PET for the assessment of lymph node metastases in prostate cancer patients with biochemical recurrence: comparison with histopathology after salvage lymphadenectomy. J Nucl Med 2016;57(11):1713–1719.
26. Schmuck S, Mamach M, Wilke F, et al. Multiple Time-Point 68Ga-PSMA I&T PET/CT for Characterization of Primary Prostate Cancer: Value of Early Dynamic and Delayed Imaging. Clin Nucl Med 2017;42(6):e286–e293.
27. Fendler WP, Schmidt DF, Wenter V, et al. 68Ga-PSMA PET/CT Detects the Location and Extent of Primary Prostate Cancer. J Nucl Med 2016;57(11):1720–1725.
28. Giesel FL, Sterzing F, Schlemmer HP, et al. Intra-individual comparison of (68)Ga-PSMA-11-PET/CT and multi-parametric MR for imaging of primary prostate cancer. Eur J Nucl Med Mol Imaging 2016;43(8):1400–1406.
29. Eiber M, Weirich G, Holzapfel K, et al. Simultaneous^{68}Ga-PSMA HBED-CC PET/MRI Improves the Localization of Primary Prostate Cancer. Eur Urol 2016;70(5):829–836.
30. Sachpekidis C, Kopka K, Eder M, et al. 68Ga-PSMA-11 Dynamic PET/CT Imaging in Primary Prostate Cancer. Clin Nucl Med 2016;41(11):e473–e479.
31. Moldovan PC, Van den Broeck T, Sylvester R, et al. What is the negative predictive value of multiparametric magnetic resonance imaging in excluding prostate cancer at biopsy? a systematic review and meta-analysis from the European Association of Urology Prostate Cancer Guidelines Panel. Eur Urol 2017;72(2):250–266.
32. Pepe P, Garufi A, Priolo G, Pennisi M. Can 3-Tesla pelvic phased-array multiparametric MRI avoid unnecessary repeat prostate biopsy in patients with PSA < 10 ng/mL? Clin Genitourin Cancer 2015;13(1):e27–e30.
33. Vinet M, Vlaeminck-Guillem V, Rouvière O, et al. Does PCA3 score and prostatic MRI help selection of patients scheduled for initial prostatic biopsy? [in French]. Prog Urol 2013;23(2):121–127.
34. Radtke JP, Kuru TH, Boxler S, et al. Comparative analysis of transperineal template saturation prostate biopsy versus magnetic resonance imaging targeted biopsy with magnetic resonance imaging-ultrasound fusion guidance. J Urol 2015;193(1):87–94.
35. Öbek C, Doğanca T, Demirci E, et al. The accuracy of^{68}Ga-PSMA PET/CT in primary lymph node staging in high-risk prostate cancer. Eur J Nucl Med Mol Imaging 2017;44(11):1806–1812.
36. Hijazi S, Meller B, Leitsmann C, et al. Pelvic lymph node dissection for nodal oligometastatic prostate cancer detected by 68Ga-PSMA-positron emission tomography/computerized tomography. Prostate 2015;75(16):1934–1940.
37. Herlemann A, Wenter V, Kretschmer A, et al. (68)Ga-PSMA positron emission tomography/computed tomography provides accurate staging of lymph node regions prior to lymph node dissection in patients with prostate cancer. Eur Urol 2016;70(4):553–557.
38. Maurer T, Gschwend JE, Rauscher I, et al. Diagnostic efficacy of (68)gallium-PSMA positron emission tomography compared to conventional imaging for lymph node staging of 130 consecutive patients with intermediate to high risk prostate cancer. J Urol 2016;195(5):1436–1443.
39. Pinaquy JB, De Clermont-Galleran H, Pasticier G, et al. Comparative effectiveness of [(18) F]-fluorocholine PET-CT and pelvic MRI with diffusion-weighted imaging for staging in patients with high-risk prostate cancer. Prostate 2015;75(3):323–331.
40. Uprimny C, Kroiss AS, Decristoforo C, et al. (68)Ga-PSMA-11 PET/CT in primary staging of prostate cancer: PSA and Gleason score predict the intensity of tracer accumulation in the primary tumour. Eur J Nucl Med Mol Imaging 2017;44(6):941–949.
41. Woythal N, Arsenic R, Kempkensteffen C, et al. Immunohistochemical validation of PSMA expression measured by 68Ga-PSMA PET/CT in primary prostate cancer. J Nucl Med 2018;59(2):238–243.
42. Uhlman MA, Sun L, Stackhouse DA, et al. Tumor volume, tumor percentage involvement, or prostate volume: which is predictive of prostate-specific antigen recurrence? Urology 2010;75(2):460–466.
43. Afshar-Oromieh A, Sattler LP, Mier W, et al. The clinical impact of additional late PET/CT imaging with^{68}Ga-PSMA-11 (HBED-CC) in the diagnosis of prostate cancer. J Nucl Med 2017;58(5):750–755.
44. Schmuck S, Nordlohne S, von Klot CA, et al. Comparison of standard and delayed imaging to improve the detection rate of [^{68}Ga]PSMA I&T PET/CT in patients with biochemical recurrence or prostate-specific antigen persistence after primary therapy for prostate cancer. Eur J Nucl Med Mol Imaging 2017;44(6):960–968.
45. Rahbar K, Ahmadzadehfar H, Kratochwil C, et al. German multicenter study investigating 177Lu-PSMA-617 radioligand therapy in advanced prostate cancer patients. J Nucl Med 2017;58(1):85–90.
46. Zechmann CM, Afshar-Oromieh A, Armor T, et al. Radiation dosimetry and first therapy results with a (124)I/ (131)I-labeled small molecule (MIP-1095) targeting PSMA for prostate cancer therapy. Eur J Nucl Med Mol Imaging 2014;41(7):1280–1292.
47. Bostwick DG, Pacelli A, Blute M, Roche P, Murphy GP. Prostate specific membrane antigen expression in prostatic intraepithelial neoplasia and adenocarcinoma: a study of 184 cases. Cancer 1998;82(11):2256–2261.